(Received 11 June 2024, Accepted 15 July 2024, Scheduled 28 July 2024)

A Novel Miniaturized Dual-Passband Half-Mode Substrate Integrated Waveguide Filter Loaded with Back-to-Back CSRR

Min Li*, Kejun Chang, and Dongya Song

Xinjiang Institute of Technology, China

ABSTRACT: In order to solve the requirements of multi-channel communication applications, this paper proposes a miniaturized dual-passband substrate integrated waveguide filter with asymmetric passband response. The design uses a half-mode substrate integrated waveguide (HMSIW) cavity, which is loaded with a back-to-back complementary open resonant ring (CSRR) according to the vanishing mode propagation theory to generate a passband response lower than the HMSIW basic mode TE_{101}, further reducing the cavity size. In addition, the band-resistive characteristics of the single-ring structure of the CSRR resonator are analyzed, and a C-slot is added at the feeder to improve the out-of-band characteristics of the second passband. Through simulation optimization and testing, the center frequency of the dual-passband filter is 4.05 GHz/8.64 GHz; the relative bandwidth is 16%/44%, the insertion loss of both passbands is better than 0.8 dB; the physical test results are consistent with the simulation ones; and the size of the filter is only $0.42\lambda_g \times 0.14\lambda_g$. It shows that the proposed filter has the characteristics of small size and low loss, and can be widely used in multi-channel RF front-end systems in the field of wireless communication.

1. INTRODUCTION

With the rapid development of wireless communication, the competition for a large number of various radio technologies and applications has become more and more fierce, and communication systems need to work in two different frequency bands, such as Global Positioning System (GPS) and 4G communication and 5G communication. Filters are an important part of RF/microwave systems, and in dual-band transceiver systems, using dual-band filters instead of two separate single-band filters can not only reduce the volume of the communication system but also save costs compared to designing a separate filter in each corresponding frequency band. In addition, higher requirements are put forward for the miniaturization, high selectivity, low loss, and multi-channel transmission capability of dual-passband filters. To meet the needs of modern communication scenarios, a new type of transmission line structure, a substrate integrated waveguide (SIW) structure, has been gradually developed and utilized. SIW structure not only has the advantages of flattening the microstrip structure and low cost, but also has the advantages of low loss and high performance of the traditional metal waveguide structure, which is very suitable for multi-channel RF front-end systems in the field of wireless communication. In recent years, many high-quality substrate-integrated filters with dual-passbands or multi-passbands have been researched and designed [1–14].

In order to achieve miniaturized and high-performance dual-passband filters, the most common methods used by scholars are: (1) loading metamaterial structures such as Complementary Split Ring Resonators (CSRRs) and Composite Right/Left-Hand (CRLH) on the cavity surface. The dual passbands are achieved by loading this electromagnetic structure in the SIW structure to generate a resonant frequency lower than the basic mode of the SIW structure [2, 15–19]; (2) Load slow-wave structures such as Defected Ground Structure (DGS) and Electromagnetic Bandgap (EBG) on the cavity surface. By etching the surface of the SIW structure to destroy the surface standard current distribution, an obvious band-stop or resonant effect is formed, to achieve dual passbands [3, 4]; (3) Add disturbed metal holes in the standard SIW cavity to change the pattern distribution in the cavity and realize the separation of different resonant modes to form dual passbands [5]; (4) Cascade coupling of resonators, etc. Different resonant cavities provide different resonant frequencies, and under the action of cascade coupling, dual passbands are formed [6, 7].

In [8], a dual-passband filter is designed using an asymmetric complementary open resonant ring. By loading a pair of asymmetric complementary resonant rings into the SIW resonator, the position parameters of the two resonant rings are changed to achieve dual passbands. However, the volume and return loss of the filter are large. Papers [9, 10] propose a method for loading groove line disturbance to form dual passbands. By loading slot line disturbance in the resonator, a new coupling structure is formed, and the overall size and stopband performance are good, but the relative bandwidth of the two passbands is small. Although a multi-resonant mode is used to implement a dual-passband filter, their bandwidth is difficult to control independently. Papers [11, 12] form dual passbands by connecting resonators of different frequencies in parallel. The resonant cavity of different frequencies makes the center frequency of the filter flexible and adjustable, but the out-of-band rejection characteristics of the filter are poor, and the volume is large. Paper [20] designs a dual-band evanescent-mode bandpass filter (BPF) on a single-layer SIW to take advantages of reduced complexity,

* Corresponding author: Min Li (minminli2022@163.com).

but higher loss and size are not favorable for signal transmission as well as system integration. In paper [21], microstrip open/short structures are used to design a dual-passband filter, but the microstrip short structures require metal vias to be realized, which will add unnecessary parasitic effects and affect the performance and stability of the filters.

In this paper, a filter design method for loading back-to-back CSRR and C-slot on HMSIW cavity is proposed. The back-to-back CSRR structure is composed of two identical and reverse-arranged CSRRs, which are used to provide the first passband lower than the cutoff frequency of the HMSIW structure, and the resonance frequency and coupling coefficient of the back-to-back CSRR are calculated by parity-mode analysis method. The corresponding coupling effect transmission curve is obtained, and two transmission zeros are formed in the lower stopband of the first passband, which realizes the degree of miniaturization and increases the frequency selectivity of the filter. The second passband is provided by the coupling of the first three modes in the HMSIW cavity, and in order to improve the out-of-band characteristics of the second passband, the resonator C-slot is etched on the top layer of the filter, and the C-slot is a single-loop structure of CSRR with band-reject characteristics, which can add an additional transmission zero point at the edge of the second passband. The test results show that the proposed design method not only reduces the size of the filter, simplifies the structural complexity, but also has high selectivity, which is very suitable for modern multi-channel communication applications.

2. THEORETICAL DESIGN AND THE PRINCIPLE OF OPERATION

2.1. HMSIW Resonator Analysis

Cutting along the midline on the SIW structure can obtain HMSIW, which has the same working mode as the SIW, but the size can be reduced by half. Therefore, HMSIW has the advantages of small size, convenient production, low cost, and easy integration in microwave millimeter wave circuits.

SIW is synthesized on a dielectric substrate using a periodic array of metallized vias, and only TE mode exists. Since the wave propagation in the SIW and rectangular metal waveguides is similar, the resonant frequency of the HMSIW cavity is:

$$f_c = \frac{c}{2\pi\sqrt{\mu\varepsilon}}\sqrt{\left(\frac{m\pi}{2L_{eff}}\right)^2 + \left(\frac{n\pi}{2W_{eff}}\right)^2} \tag{1}$$

where (1): $m, n = 1, 2, 3\ldots$; c is the propagation speed of electromagnetic waves in a vacuum; ε and μ are the dielectric constant and permeability of the dielectric substrate, respectively; L_{eff} and W_{eff} are the equivalent length and equivalent width of HMSIW, respectively, as follows:

$$L_{eff} = L - \frac{d^2}{0.95p} \tag{2}$$

$$W_{eff} = W - \frac{d^2}{0.95p} \tag{3}$$

In Equations (2) and (3): p, d and L, W are, respectively, the spacing, diameter and length, width of the SIW structure of the metalized vias. When, $d/p > 0.5$, $d/\lambda < 0.1$ satisfied, the magnetic wall composed of metal vias hardly causes electromagnetic leakage.

Figure 1 shows the structure diagram of the initial half-mode substrate integrated waveguide (HMSIW). To study the transmission characteristics of the HMSIW structure, the eigenmode simulation of the structure by the simulation software HFSS is used, and the electric field distribution of the first three resonant modes in the HMSIW cavity is given in Fig. 2. In Fig. 2(a), the resonant frequency corresponding to the main mode TE_{101} of the HMSIW cavity is 5.97 GHz, and it is also the cutoff frequency of the HMSIW structure. Figs. 2(b) and (c) show the two higher-order modes TE_{201} and TE_{103}, corresponding to 7.68 GHz and 9.12 GHz, respectively, and at this time, the three mode resonance points in the HMSIW cavity are close to each other and can be used to provide a passband of the filter.

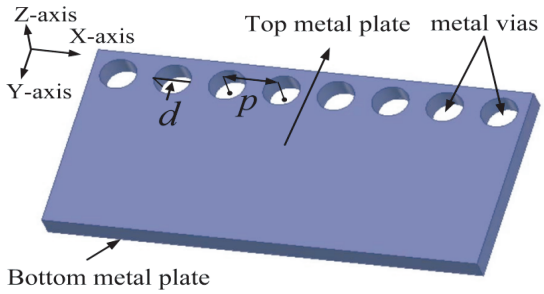

FIGURE 1. HMSIW structure.

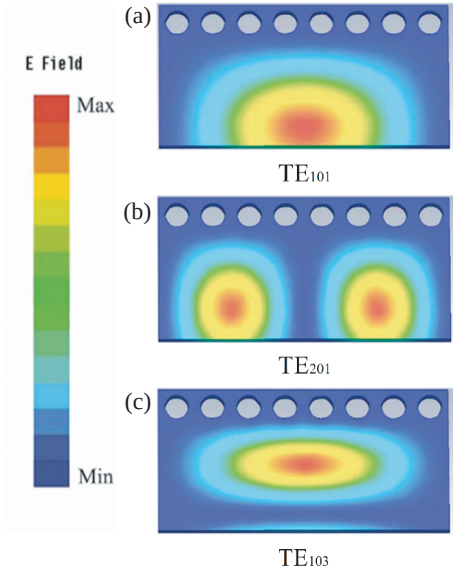

FIGURE 2. HMSIW cavity electric field distribution. (a) 5.97 GHz (the TE_{101} mode). (b) 7.68 GHz (the TE_{201} mode). (c) 9.12 GHz (the TE_{103} mode).

2.2. Back-to-Back CSRR Resonator Structure

Using the low-frequency bandpass transmission characteristics of conventional CSRR, it is possible to add a passband at a low

frequency without increasing the filter volume, and realize a miniaturized design. Compared with the traditional coupled CSRR, the coupling strength of the back-to-back CSRR structure is more controllable, which can greatly affect the electric field distribution in the resonant cavity and is convenient for the design and adjustment of the passband.

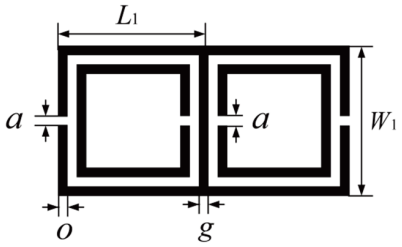

FIGURE 3. Back-to-back CSRR unit structure.

As shown in Fig. 3, back-to-back CSRR is formed by a pair of identical CSRR structures arranged side by side in reverse, and CSRR can be achieved by nesting two open rings of different sizes, whose equivalent circuit is shown in Fig. 4. Since there is no gap between back-to-back CSRRs, they can be tightly coupled to each other, and the coupling between two independent CSRRs is electromagnetic coupling. Electrical coupling and magnetic coupling work together as a pair of electric dipoles under axial electric field excitation and work near the resonant frequency. In Fig. 4, the self-inductance and self-capacitance equivalent to two independent CSRR structures are equivalent to the mutual inductance and mutual capacitance between back-to-back CSRRs [15–18].

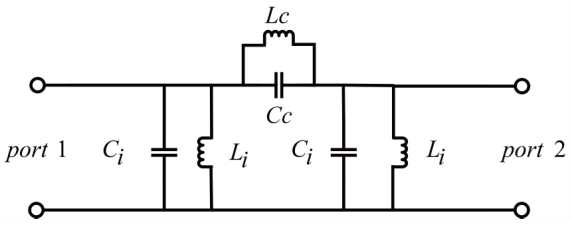

FIGURE 4. Back-to-back CSRR equivalent circuit.

3. BACK-TO-BACK CSRR-HMSIW TRANSMISSION RESPONSE

The back-to-back CSRR is loaded onto the upper metal surface of the HMSIW cavity to form a back-to-back CSRR-HMSIW structure, as shown in Fig. 5.

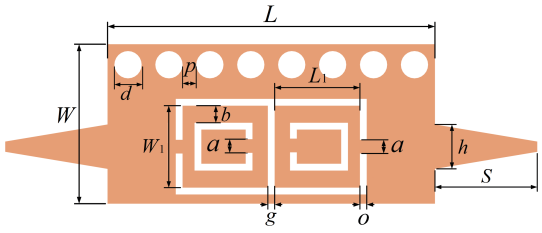

FIGURE 5. Back-to-back CSRR-HMSIW structure.

The diameter of HMSIW waveguide metal vias is 0.8 mm, and the distance between adjacent vias is 1.2 mm. The electromagnetic field simulation software HFSS 15.0 was used to analyze the back-to-back CSRR-HMSIW resonator structure and the transmission characteristics of HMSIW structure, and the corresponding transmission characteristic curve is shown in Fig. 6.

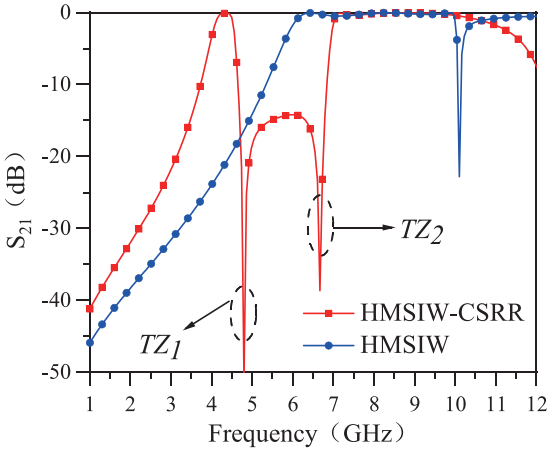

FIGURE 6. Back-to-back CSRR-HMSIW transmission characteristic curve.

As can be seen from Fig. 6, the HMSIW cavity is loaded with back-to-back CSRRs, forming another passband below the HMSIW cavity cutoff frequency. The back-to-back CSRR structure produces a passband center frequency of 4.25 GHz, a relative bandwidth of 18%, and an in-passband insertion loss of less than 0.3 dB.

Since there are no gaps between the two CSRR structures, this configuration can result in transmission zero points on each side of the passband. It is clear that there are two pathways from the input to the output through the two CSRRs, which act as two resonators in this filter. Two transmission zeros emerge from the two pathways' opposing phase shifts. At the same time, there is a higher level of out-of-band inhibition. Since the waveguide has a cutoff frequency of 5.97 GHz and the resonant frequency shifts to a lower frequency after adopting a back-to-back CSRR structure, the conventional HMSIW filter is miniaturized by 42.6%.

SIW metal vias are equivalent to inductors by array modeling L_d. Input coupling includes electrical coupling and magnetic coupling, which are expressed as L_r and C_r. The equivalent circuit model diagram of the resulting back-to-back CSRR-HMSIW filter is shown in Fig. 7(a). The resonance characteristics of odd mode and even mode analysis were studied, and the odd mode and even-mode equivalent circuit diagrams shown in Figs. 7(b) and (c) were used to derive odd mode and even-mode input admittance Y_{ino} and Y_{ine} as shown in Equations (4) and (5).

$$Y_{\text{ino}} = -\frac{j}{\omega L_d} + \frac{\left(-\frac{j}{\omega L_r} + j\omega C_r\right)\left(-\frac{j}{\omega L_i} + j\omega C_i\right)}{-\frac{j}{\omega}\left(\frac{1}{L_r} + \frac{1}{L_i}\right) + j\omega\left(C_r + C_i\right)} \tag{4}$$

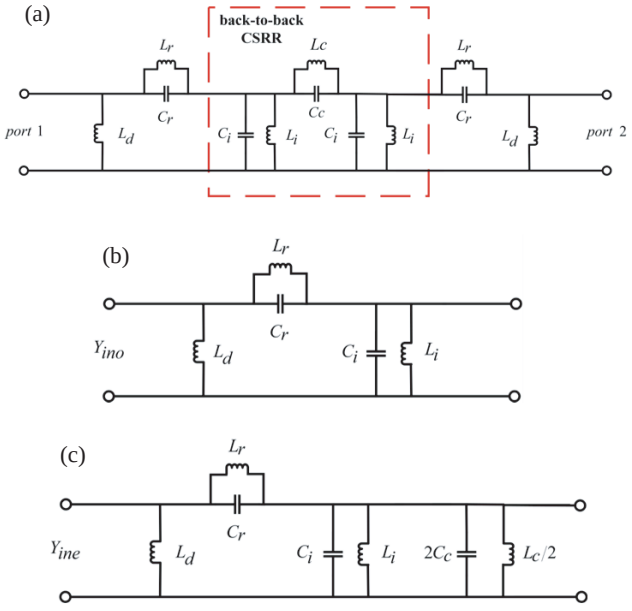

FIGURE 7. (a) Equivalent circuit of Back to back CSRR filter; (b) Odd mode Equivalent circuit; (c) Even mode Equivalent circuit. (L_c = 1.36 nH, C_c = 0.613 pF, L_i = 0.565 nH, C_i = 1.48 pF, L_r = 0.496 nH, C_r = 0.492 pF).

$$Y_{\text{ine}} = -\frac{j}{\omega L_d} + \frac{\left(-\frac{j}{\omega L_r} + j\omega C_r\right)}{\frac{\left[-\frac{j}{\omega}\left(\frac{1}{L_i}+\frac{2}{L_c}\right)+j\omega\left(C_i+2C_c\right)\right]}{-\frac{j}{\omega}\left(\frac{1}{L_r}+\frac{1}{L_i}+\frac{2}{L_c}\right)+j\omega\left(C_r+C_i+2C_c\right)}} \quad (5)$$

When the odd mode and even mode transmission poles are close to infinity, the resonant frequencies f_{odd} and f_{even} of odd mode and even mode are shown in Equations (6) and (7):

$$f_{\text{odd}} = \frac{\sqrt{L_i + L_r}}{2\pi\sqrt{L_r L_i\left(C_r + C_i\right)}} \quad (6)$$

$$f_{\text{even}} = \frac{\sqrt{L_i L_c + L_r L_c + 2L_r L_i}}{2\pi\sqrt{L_r L_i L_c\left(C_r + C_i + 2C_c\right)}} \quad (7)$$

From Equations (6) and (7), it can be seen that only the even-mode resonant frequency is affected by the intercoupling elements L_c and C_c. The electromagnetic simulation method is used to study, and the coupling coefficient is extracted as shown in Equation (8):

$$K = \frac{\left|f_{\text{odd}}^2 - f_{\text{even}}^2\right|}{f_{\text{odd}}^2 - f_{\text{even}}^2} \quad (8)$$

According to the strength of the coupling coefficient between the two resonant elements, the resulting coupling effect can strengthen or weaken the energy storage of the resonant ring at the operating frequency. From Equation (7) and Equation (8), it can be seen that the coupling coefficient K between back-to-back CSRRs is mainly affected by the mutual capacitance C_c between the two CSRRs. As can be seen from Fig. 7(a), the larger the width of the gap g between the back-to-back CSRRs is, the greater the mutual capacitance C_c of the equivalent circuit is.

Figure 8 shows the influence of adjusting the width of the gap g between back-to-back CSRRs on the coupling coefficient K and odd-mode and even-mode resonant frequencies. As shown in Fig. 8, as the gap g width between back-to-back CSRRs increases, the coupling coefficient K gradually decreases, and the even-mode resonant frequency gradually increases. It is verified that the even-mode resonant frequency is more sensitive to the change of mutual capacitance C_c, while the change of odd-mode resonant frequency is negligible.

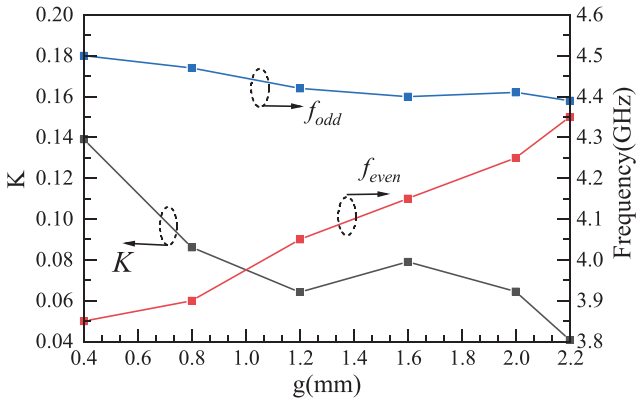

FIGURE 8. Influence of g on odd and even mode frequency and coupling coefficient.

When $Y_{\text{ino}} = Y_{\text{ine}}$, transmitting the zero point, as shown in Equations (9) and (10):

$$Z_{\text{T1}} = \frac{1}{2\pi\sqrt{L_c C_c}} \quad (9)$$

$$Z_{\text{r2}} = \frac{1}{2\pi\sqrt{L_r C_r}} \quad (10)$$

4. LOAD THE C-SLOT

In order to improve the lower stopband suppression characteristics of the second passband, two symmetrical C-slots are loaded on the back-to-back CSRR-HMSIW structure. The structure is shown in Fig. 9.

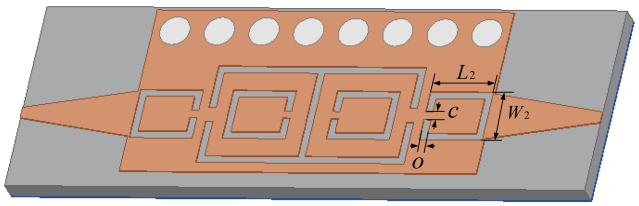

FIGURE 9. Back-to-back CSRR-HMSIW structure.

CSRR as a duality argument for an open resonant ring (SRR) has been shown to have a negative permittivity constant. Since the signal cannot propagate near its resonant frequency, CSRR has stopband performance. The C-slot designed in this section adopts a CSRR single-ring structure, and the induced current

TABLE 1. Filter size parameters (unit: mm).

Parameters	Value (mm)	Parameters	Value (mm)	Parameters	Value (mm)
L	31.2	W	10.4	g	0.60
L_1	11.2	W_1	5.60	h	0.40
L_2	3.40	W_2	2.80	o	0.40
a	0.40	b	0.40	p	1.20
c	0.20	d	0.80	s	6.00

generated under the action of the electromagnetic field will also change the original magnetic field distribution, to suppress a certain frequency, so the C-slot also has the same stopband performance.

In the simulation software, the opening length of the C-slot has a great influence on the stop-band suppression characteristics under the second passband, and the size of the C-slot opening length is changed. The corresponding transmission characteristic curve is shown in Fig. 10.

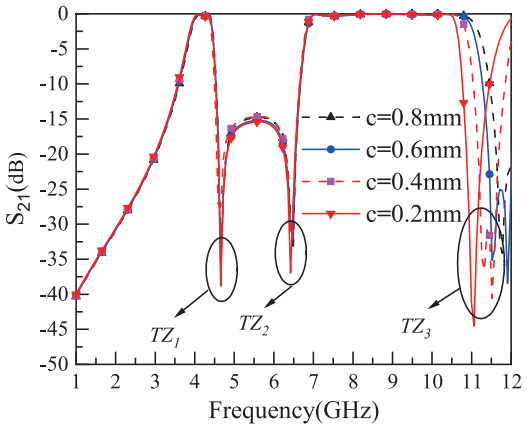

FIGURE 10. Influence of c on out-of-band suppression.

When the C-slot opening length c becomes larger, its resonant frequency becomes higher, creating a parasitic passband outside the second passband. When c is 0.2 mm, the resonant frequency is located at the high frequency of the passband range generated by the HMSIW structure, and the out-of-band characteristic of the C-slot structure itself will generate a new transmission zero TZ_3 at the lower resistance band of the second passband. The final C-slot opening length c is determined to be 0.2 mm.

5. PROCESSING AND TEST RESULTS

In order to optimize the transmission characteristics of the designed filter, the final size of the filter structure is shown in Table 1 after simulation and optimization.

In order to verify the feasibility of back-to-back CSRR miniaturized dual-passband filters, a standard printed circuit board (PCB) process was used to make a substrate of Rogers 5880 material with a dielectric constant of 2.2 and a thickness of 1.016 mm. Fig. 11 shows the actual processing diagram of the filter, which has dimensions of $0.42\lambda_g \times 0.14\lambda_g$. Using the

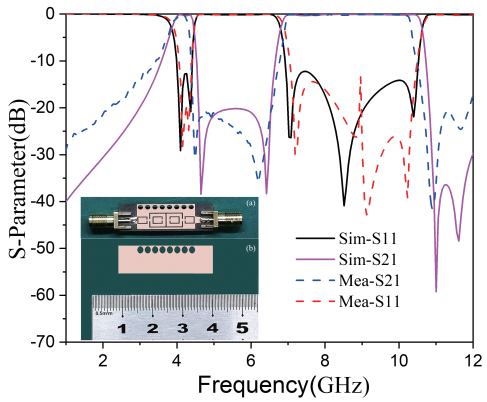

FIGURE 11. Comparison of test results and simulation results. (a) Front view. (b) Back view.

Agilent N5242A vector network analyzer for testing, Fig. 11 displays the simulated findings as well as the measured data.

The measured center frequencies are 4.05 GHz and 8.64 GHz, corresponding to relative bandwidths of 16% and 44%, respectively, and the maximum interpolation loss score in the band.

The return loss is 23 dB and 16 dB, respectively. Three transmission zeros are generated outside the passband, and the isolation between the two passbands can approach 35 dB. The high band's 6.80 GHz ~ 10.67 GHz rejection is larger than 38 dB. As can be observed from Fig. 11, there are three main explanations for why the measured in-band insertion loss, return loss, and isolation between the two passbands of the filter differ from the simulation results. First, radiation takes place inside the waveguide in a plane parallel to the ground, with through-wall restriction. Second, because this research uses a structure with slot coupling rather than a completely closed structure, the filter exhibits a significant radiation loss. The device's processing mistake, metal loss, loss of the SMA connector, etc. will also have an effect to some degree on the measured data. The test findings largely agree with the modeling, showing that the suggested filter is capable of high selectivity and dual passbands.

The filter designed in this study is contrasted with some other recent designs that are similar in order to highlight the properties of the filter's small size and low loss in Table 2. It can be shown from comparisons that the suggested filter offers a lot of advantages in terms of construction size and transmission properties. The filter developed in this work performs well overall and has a smaller size and higher selectivity than some previous studies.

TABLE 2. This filter is compared with those of other filters.

Ref.	Center frequency (GHz)	IL (dB)	RL (dB)	FBW (%)	No. of TZs	Size $\lambda^2 g$	ε_r
[3]	5.83/18.1	1.62/6.39	20.0/35.0	9.77%/4.09%	4	0.86×0.25	2.2
[5]	13.0/14.0	2.86/3.37	22.0/10.0	2.14%/1.79%	3	3.32×1.16	2.38
[12]	5.30/8.50	2.02/1.82	15.0/21.0	6.26%/7.75%	4	1.31×0.84	2.2
[22]	6.22/8.24	0.86/1.32	25.0/23.0	7.70%/3.90%	3	0.89×0.41	2.38
[23]	33.6/38.0	5.00/2.20	12.0/10.0	2.68%/3.68%	1	1.05×0.63	2.2
This work	4.05/8.64	0.80/0.60	23.0/16.0	16.0%/44.0%	3	0.42×0.14	2.2

6. CONCLUSION

In this paper, a back-to-back CSRR structure is studied. The transmission characteristics of the back-to-back CSRR structure are systematically analyzed, and dual passbands combined with the HMSIW structure to reduce the filter volume by 46.6%. Three transmission zeros are generated, which enhances the filter's frequency selectivity. In addition, according to the band-resistive characteristics of the CSRR single-ring structure, a symmetrical C-slot is designed to significantly improve the out-of-band characteristics. In order to verify the feasibility of the design method, a miniaturized dual-passband SIW filter was designed, manufactured, and tested. The proposed filter has the characteristics of small size, low insertion loss, and high-frequency selectivity, which can be used in communication equipment integrated circuits, and broadens the design path of multi-passband filters.

ACKNOWLEDGEMENT

This work was supported by Xinjiang "Tianchi Talents" Introduction Program (No:2023TCLJ03).

REFERENCES

[1] Song, K., Y. Zhu, and F. Zhang, "Single-and dual-band filtering-response power dividers embedded SIW filter with improved output isolation," *Scientific Reports*, Vol. 7, No. 1, 3361, 2017.

[2] Jiang, D., Y. Liu, X. Li, G. Wang, and Z. Zheng, "Tunable microwave bandpass filters with complementary split ring resonator and liquid crystal materials," *IEEE Access*, Vol. 7, 126 265–126 272, 2019.

[3] Pelluri, S. and M. V. Kartikeyan, "Widely separated dual-band half-mode SIW bandpass filter," *International Journal of RF and Microwave Computer-Aided Engineering*, Vol. 30, No. 10, e22360, 2020.

[4] Hinojosa, J., M. Rossi, A. Saura-Ródenas, A. Álvarez Melcón, and F. L. Martínez-Viviente, "Compact bandstop half-mode substrate integrated waveguide filter based on a broadside-coupled open split-ring resonator," *IEEE Transactions on Microwave Theory and Techniques*, Vol. 66, No. 6, 3001–3010, 2018.

[5] Xie, H.-W., K. Zhou, C.-X. Zhou, and W. Wu, "Compact wide-stopband SIW dual-band filter with closely spaced passbands," *Electronics Letters*, Vol. 56, No. 16, 822–825, 2020.

[6] Zhou, K., C.-X. Zhou, H.-W. Xie, and W. Wu, "Synthesis design of SIW multiband bandpass filters based on dual-mode resonances and split-type dual-and triple-band responses," *IEEE Transactions on Microwave Theory and Techniques*, Vol. 67, No. 1, 151–161, 2018.

[7] Zhu, Y. and Y. Dong, "Novel double-layer SIW filter with mechanically adjustable frequency response," *IEEE Microwave and Wireless Components Letters*, Vol. 31, No. 4, 357–360, 2021.

[8] Yin, B., Q.-Q. Huang, X.-L. Zhang, J.-L. Liu, J.-H. Xia, Y.-Y. Zhang, and J.-R. Liang, "Bandpass filters combined siw with asymmetric circle complementary spilt-ring resonator," *Chinese Jounal of Electron Devices*, Vol. 44, No. 05, 1072–1077, 2021.

[9] Yin, B., X. Cai, and S. Zhang, "Design of compact crlh bandpass filter based on structure of CSRR-SIW," *Journal of Chongqing University of Posts and Telecommunications (Natural Science Edition)*, Vol. 30, No. 2, 243–248, 2018.

[10] Liu, B.-G., Y.-P. Lyu, L. Zhu, and C.-H. Cheng, "Compact single- and dual-band filters on hexa-modes half-mode substrate integrated waveguide resonator with loaded H-shaped slot," *IEEE Microwave and Wireless Components Letters*, Vol. 30, No. 12, 1129–1132, 2020.

[11] Muchhal, N. and S. Srivastava, "Design of miniaturized diamond shaped substrate integrated waveguide CSRR band pass filter for X band applications," in *2019 International Conference on Signal Processing and Communication (ICSC)*, 113–116, Noida, India, 2019.

[12] Zhou, K., C.-X. Zhou, and W. Wu, "Dual-mode characteristics of half-mode SIW rectangular cavity and applications to dual-band filters with widely separated passbands," *IEEE Transactions on Microwave Theory and Techniques*, Vol. 66, No. 11, 4820–4829, 2018.

[13] Wu, J., Y. Huang, and Z. Xue, "Coplanar waveguide dual-passband filter based on zero-degree feed," *Electronic Components & Materials*, Vol. 46, No. 10, 1227–1231, 2023.

[14] Li, D., C. Wang, X. Cui, D. Chen, C. Fei, and Y. Yang, "Recent progress and development of interface integrated circuits for piezoelectric energy harvesting," *Nano Energy*, Vol. 94, 106938, 2022.

[15] Shi, L.-F., C.-Y. Sun, S. Chen, G.-X. Liu, and Y.-F. Shi, "Dual-band substrate integrated waveguide bandpass filter based on CSRRs and multimode resonator," *International Journal of RF and Microwave Computer-Aided Engineering*, Vol. 28, No. 9, e21412, 2018.

[16] Zheng, Y. and Y. Dong, "Miniaturized hybrid filter using stripline and LC-loaded SIW resonators," *IEEE Transactions on Circuits and Systems II: Express Briefs*, Vol. 69, No. 9, 3719–3723, 2022.

[17] Zhang, H., W. Kang, and W. Wu, "Miniaturized dual-band differential filter based on CSRR-loaded dual-mode SIW cavity," *IEEE Microwave and Wireless Components Letters*, Vol. 28, No. 10, 897–899, 2018.

[18] Gao, M., M. Li, J. Nan, and Y. Wang, "New dual-passband SIW filter with loaded T-slot," *Progress In Electromagnetics Research C*, Vol. 124, 243–252, 2022.

[19] Liang, J. and W.-H. Liao, "Improved design and analysis of self-powered synchronized switch interface circuit for piezoelectric energy harvesting systems," *IEEE Transactions on Industrial Electronics*, Vol. 59, No. 4, 1950–1960, 2011.

[20] Nosrati, A., M. Mohammad-Taheri, and M. Nosrati, "Gap-coupled dual-band evanescent-mode substrate integrated bandpass filter waveguide," *Progress In Electromagnetics Research Letters*, Vol. 89, 53–59, 2020.

[21] Shen, H., J. Qiu, H. Ji, K. Zhu, and M. Balsi, "Enhanced synchronized switch harvesting: A new energy harvesting scheme for efficient energy extraction," *Smart Materials and Structures*, Vol. 19, No. 11, 115017, 2010.

[22] Xu, S., K. Ma, F. Meng, and K. S. Yeo, "Novel defected ground structure and two-side loading scheme for miniaturized dual-band SIW bandpass filter designs," *IEEE Microwave and Wireless Components Letters*, Vol. 25, No. 4, 217–219, 2015.

[23] He, Z., Z. Shao, X. Li, and M. Shen, "A dual-band bandpass filter based on hybrid structure of substrate integrated waveguide and substrate integrated coaxial line," in *2016 IEEE MTT-S International Microwave Symposium (IMS)*, 1–4, San Francisco, CA, USA, 2016.